

FTF-ER: Feature-Topology Fusion-Based Experience Replay Method for Continual Graph Learning

Jinhui Pang
Beijing Institute of Technology
Beijing, China
pangjinhui@bit.edu.cn

Changqing Lin
Beijing Institute of Technology
Beijing, China
lcq2000@bit.edu.cn

Xiaoshuai Hao*
Samsung Rearch China-Beijing
Beijing, China
xshuai.hao@samsung.com

Rong Yin
Institute of Information Engineering,
Chinese Academy of Sciences
Beijing, China
yinrong@iie.ac.cn

Zixuan Wang
Beijing Institute of Astronautical
Systems Engineering
Beijing, China
ZixuanWang0802@163.com

Zhihui Zhang
Beijing Institute of Technology
Beijing, China
3220231441@bit.edu.cn

Jinglin He
Beijing Institute of Technology
Beijing, China
hozyelflin01@gmail.com

Huang Tai Sheng
Beijing Institute of Technology
Beijing, China
3820221088@bit.edu.cn

Abstract

Continual graph learning (CGL) is an important and challenging task that aims to extend static GNNs to dynamic task flow scenarios. As one of the mainstream CGL methods, the experience replay (ER) method receives widespread attention due to its superior performance. However, existing ER methods focus on identifying samples by feature significance or topological relevance, which limits their utilization of comprehensive graph data. In addition, the topology-based ER methods only consider local topological information and add neighboring nodes to the buffer, which ignores the global topological information and increases memory overhead. To bridge these gaps, we propose a novel method called **Feature-Topology Fusion-based Experience Replay (FTF-ER)** to effectively mitigate the catastrophic forgetting issue with enhanced efficiency. Specifically, from an overall perspective to maximize the utilization of the entire graph data, we propose a highly complementary approach including both feature and global topological information, which can significantly improve the effectiveness of the sampled nodes. Moreover, to further utilize global topological information, we propose Hodge Potential Score (HPS) as a novel module to calculate the topological importance of nodes. HPS derives a global node ranking via Hodge decomposition on graphs, providing more accurate global topological information compared to neighbor sampling. By excluding neighbor sampling, HPS significantly reduces buffer

storage costs for acquiring topological information and simultaneously decreases training time. Compared with state-of-the-art methods, FTF-ER achieves a significant improvement of 3.6% in AA and 7.1% in AF on the OGB-Arxiv dataset, demonstrating its superior performance in the class-incremental learning setting.

CCS Concepts

• **Mathematics of computing** → **Graph algorithms**; • **Computing methodologies** → **Neural networks**.

Keywords

Continual Graph Learning, Experience Replay, Hodge Decomposition

ACM Reference Format:

Jinhui Pang, Changqing Lin, Xiaoshuai Hao, Rong Yin, Zixuan Wang, Zhihui Zhang, Jinglin He, and Huang Tai Sheng. 2024. FTF-ER: Feature-Topology Fusion-Based Experience Replay Method for Continual Graph Learning. In *Proceedings of the 32nd ACM International Conference on Multimedia (MM '24)*, October 28–November 1, 2024, Melbourne, VIC, Australia. ACM, New York, NY, USA, 12 pages. <https://doi.org/10.1145/3664647.3681457>

1 Introduction

Continual learning (CL) in the field of graph neural networks (GNNs) [11, 19, 32] has become increasingly significant due to its potential applications in dynamic and evolving environments. Traditional GNN models are designed to operate on static graph data, making them inadequate for scenarios where graphs evolve over time. Continual graph learning (CGL) addresses this challenge by extending GNNs to adapt to changing graph structures and data distributions [38]. This enables models to continuously learn and update their knowledge without forgetting previous information. The ability to learn from sequential data and adapt to new dynamic information is crucial for various real-world applications such as social network analysis [12], recommendation systems [10] and traffic prediction [7]. In this context, developing effective continual

*Corresponding author.

Permission to make digital or hard copies of all or part of this work for personal or classroom use is granted without fee provided that copies are not made or distributed for profit or commercial advantage and that copies bear this notice and the full citation on the first page. Copyrights for components of this work owned by others than the author(s) must be honored. Abstracting with credit is permitted. To copy otherwise, or republish, to post on servers or to redistribute to lists, requires prior specific permission and/or a fee. Request permissions from permissions@acm.org.
MM '24, October 28–November 1, 2024, Melbourne, VIC, Australia

© 2024 Copyright held by the owner/author(s). Publication rights licensed to ACM.
ACM ISBN 979-8-4007-0686-8/24/10
<https://doi.org/10.1145/3664647.3681457>

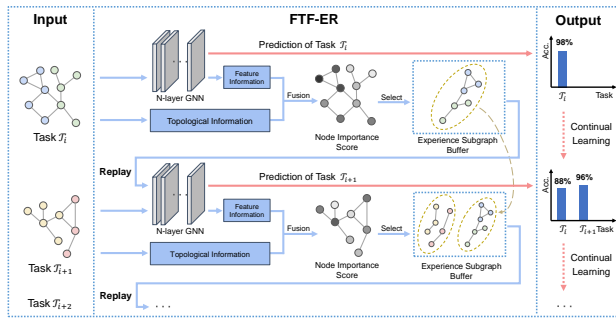


Figure 1: FTF-ER workflow: Nodes are selected from each class based on importance scores to create induced subgraphs for the buffer. This enables the model to maintain classification performance across tasks, i.e., continual learning.

learning strategies for graphs has emerged as a key research area with the aim of enhancing the robustness and adaptability of GNN models in dynamic environments.

CGL methods can be categorized into three classes [48]: regularization methods, parametric isolation methods and experience replay (ER) methods. Among them, ER methods, inspired by the complementary learning systems theory in cognitive science [21, 27], have achieved SOTA performance in both traditional CL and CGL fields. To help the model stay good at the earlier tasks, ER methods use a partial collection of training samples from previous tasks and reintroduce them when training on new tasks. In recent years, some studies integrate ER methods to deal with the issue of graph learning in streaming scenarios [38]. ER-GNN [50] stores representative nodes at the feature level for experience replay. SGNN-GR [39] incorporates generative replay to learn and generate fake historical samples. Recently, SSM [49] stores sparsified subgraphs to gain topological-level experience and achieves SOTA performance in CGL. However, the ER methods mentioned above primarily select impactful samples based on either feature significance or topological relevance, which limits their utilization of the comprehensive graph data. Furthermore, to provide local topological information, SSM expands the buffer by adding nodes that are not present in the experience samples, resulting in the neglect of global topological information and the requirements of additional storage.

To address the aforementioned issues, we integrate information from both the feature and topological levels and propose a novel experience replay method called Feature-Topology Fusion-based Experience Replay (FTF-ER¹) to mitigate the catastrophic forgetting issue in CGL. Figure 1 shows the workflow of FTF-ER, and the essence of the workflow centers on the approach to acquiring information for sampling. Specifically, we employ two theoretically grounded approaches to calculate the feature-level and topological-level importance scores of nodes. Firstly, inspired by [28], we use gradient norm score (GraNd) to compute the node importance in the feature space. GraNd measures the importance of a node by evaluating the change in the loss of all other nodes when the node is added to the training set. Furthermore, we propose Hodge potential score (HPS) as a novel module to calculate the topological importance

of nodes by using Hodge decomposition on graphs (HDG) [17, 23]. HDG is an effective tool for studying the topological properties of nodes that can establish a natural and computable node potential function. This function can derive a global ranking from pairwise comparison relationships among all nodes. It explicitly highlights the global topological importance of each node. To the best of our knowledge, our study represents the first application of HDG to node importance computation. By precomputing the HPS of nodes before training, our method efficiently captures comprehensive global topological information in the node sampling phase. HPS enhances the accuracy of topological information while eliminating the need for additional nodes during the subgraph creation phase.

In summary, our contributions can be outlined as follows:

- We present Feature-Topology Fusion-based Experience Replay (FTF-ER), a novel framework from an overarching standpoint, which aims to efficiently and effectively alleviate the catastrophic forgetting problem in continual graph learning.
- To fully utilize the comprehensive graph data, we propose an integrative approach to better represent node importance. We first normalize the node importance scores on features and topology separately, and then obtain the aggregated importance by calculating the weighted average of two scores, thereby improving the accuracy of node importance.
- We propose Hodge potential score (HPS), a preprocessing module to capture global topological information without adding neighboring nodes to the buffer. Consequently, HPS further utilizes global topological information and reduces buffer storage costs of topology-based ER methods.
- We conduct extensive experiments on four mainstream graph datasets, and achieve state-of-the-art performance on accuracy, time efficiency in the class-incremental learning setting. Moreover, despite leveraging topological information, our buffer storage costs are comparable to topology-agnostic methods.

2 Related work

2.1 Experience Replay

Continual graph learning seeks to sequentially train the model as graph data from various tasks are received in a stream. Similar to continual learning research in other fields [14–16, 30], research methods for CGL can be mainly categorized into three major types [47]. The first family consists of regularization methods that focus on preserving the parameters inferred in one task while training on another [1, 8, 20, 22, 24]. The second family is parametric isolation methods that separate parameters from different tasks explicitly [31, 41, 44, 45]. The last family is experience replay methods that store a limited amount of representative data from previous tasks and replay them during training on subsequent tasks in order to maintain the model’s ability to classify past tasks [2, 25, 29]. As an illustration, Gradient Episodic Memory (GEM) [25] constrains the gradient of the current task to prevent an increase in the loss associated with the data stored in episodic memory. In the domain of graphs, Experience Replay Graph Neural Network (ER-GNN) [50] stores representative nodes at the feature level for experience replay, while Sparsified Subgraph Memory (SSM) [49] stores sparsified subgraphs that include k -hop neighboring nodes to gain local

¹Codes are available at <https://github.com/CyanML/FTF-ER>

topological-level experience. However, previous methods primarily have two drawbacks: (1) They select samples based on either feature significance or topological relevance, limiting their comprehensive utilization of graph data. (2) SSM adds neighboring nodes to the buffer, overlooking global topological information and increasing storage needs. Different from them, our FTF-ER combines both feature and topological information of nodes to provide an overall perspective for alleviating the catastrophic forgetting problem. Furthermore, we propose Hodge potential score to obtain global topological information without introducing extra nodes, thereby further utilizing global topological information and reducing the buffer storage overhead of topology-based ER methods.

2.2 Application of Hodge Decomposition

In the realm of machine learning, Hodge decomposition has found several innovative applications, serving as a foundational tool for understanding complex data structures through the lens of algebraic topology [5, 13, 33, 34]. For example, previous work [36] develops a set of tools for analyzing 3D discrete vector fields on tetrahedral grids using a Hodge decomposition approach. In addition, researchers apply Hodge decomposition to robustly find global rankings in the presence of outliers for image processing [46]. In the field of robotics, Helmholtz-Hodge decomposition is used to create algorithms that approximate incompressible flows for agent control and stream function computation in graph-modeled environments [18]. In [17] and [23], researchers introduce Hodge decomposition on graphs (HDG) and apply it to statistical ranking problems. Furthermore, in [43], researchers use HodgeRank for paired comparison data in the multimedia domain, assessing video quality and analyzing inconsistencies. For the advantage of Hodge decomposition's ability to reliably and globally rank nodes in graphs with robustness, even among irregular data, it has seen widespread application in various fields. To the best of our knowledge, we first introduce HDG to the field of continual graph learning, thus obtaining global topological information and reducing buffer storage requirements of topology-based ER methods.

3 Method

3.1 Preliminaries

Notations. For a graph $\mathcal{G} = (\mathcal{V}, \mathcal{E})$ with n nodes, we have a node set $\mathcal{V} = \{v_1, v_2, \dots, v_n\}$ and an edge set $\mathcal{E} = \{(u, v) | u \in \mathcal{V}, v \in \mathcal{V}\}$. We use the adjacency matrix $\mathbf{A} \in \mathbb{R}^{n \times n}$ to describe the connectivity of \mathcal{G} , and each non-zero element in \mathbf{A} corresponds to an edge in \mathcal{E} . In this paper, we study the node classification problem in which each node $v \in \mathcal{V}$ has a category label $y^l \in \mathcal{Y}$ where $\mathcal{Y} = \{y^1, y^2, \dots, y^c\}$ is the label set and c is the number of classes. GNNs are the mainstream solution for node classification problems.

Problem Definition. In this paper, we focus on the continual graph node classification problem. In a learning process, the model is continually trained on a sequence of disjoint tasks $\mathcal{T} = \{\mathcal{T}_1, \mathcal{T}_2, \dots, \mathcal{T}_K\}$, where K represents the number of tasks. Each task \mathcal{T}_i comprises multiple non-overlapping classes $\mathcal{Y}_i = \{y^1, y^2, \dots, y^{c_i}\}$ and c_i is the number of classes in task \mathcal{T}_i . We define the node set of \mathcal{T}_i as $\mathcal{V}_i = \{v | y(v) \in \mathcal{Y}_i, v \in \mathcal{V}\}$, where $y(v)$ is the label of node v . Then the induced subgraph of \mathcal{T}_i can be represented as $\mathcal{G}_i =$

$(\mathcal{V}_i, \mathcal{E}_i)$, $\mathcal{E}_i = \{(u, v) | u, v \in \mathcal{V}_i, (u, v) \in \mathcal{E}\}$. In the continual learning settings, different tasks correspond to different induced subgraphs without overlap on \mathcal{Y} . Once the learning of a task is completed, the vast majority of the training data related to this task are no longer available. The goal of CGL is to achieve consistent high performance across all tasks in the sequence, addressing both current task performance and mitigating the catastrophic forgetting problems for past tasks.

Incremental Learning Settings. Continual learning has two main settings: task-incremental learning (task-IL) and class-incremental learning (class-IL). The key difference lies in whether task indicators are provided to the model during testing. In task-IL, the model receives a task indicator, enabling it to concentrate solely on the classes relevant to the current task during classification. Conversely, in class-IL, the model must identify all previously learned classes without the assistance of task indicators. Class-IL is considered more challenging due to the larger classification dimension and the absence of explicit task boundaries. Previous studies [48] have shown that CGL methods significantly perform better in task-IL than in class-IL. In this paper, we aim to tackle the more challenging class-IL tasks to showcase the effectiveness of our method.

3.2 Experience Replay on Subgraphs

In the field of graphs, due to the presence of rich topological structures, experience replay (ER) methods can be extended to ER on subgraphs. The traditional ER methods preserve a small number of training samples from past tasks and replay them during the subsequent tasks training in order to retain the model's classification ability for past tasks. The key to ER methods lies in designing a rational experience sample selection strategy. Previous research has revealed that samples are inherently unequal; some samples may carry information that can significantly improve model performance, while the addition of other samples may have little impact on enhancing model effectiveness [35]. For a given task \mathcal{T}_k and its training dataset \mathcal{D}_k^{tr} , ER methods use an experience sample strategy $\mathcal{S}(\cdot)$ to collect experience samples from \mathcal{D}_k^{tr} and add them to the experience buffer \mathcal{B} . A simple way to replay the experience in \mathcal{B} is applying an auxiliary loss:

$$\mathcal{L} = \sum_{x_i \in \mathcal{D}_k^{tr}} l(f(x_i; \theta), y_i) + \lambda \sum_{x_j \in \mathcal{B}} l(f(x_j; \theta), y_j), \quad (1)$$

where $l(\cdot, \cdot)$ denotes the loss function, $f(\cdot; \theta)$ denotes the model training on the task sequence, and λ is utilized to balance the auxiliary loss. When training $f(\cdot; \theta)$ in \mathcal{T}_k , \mathcal{B} contains the experience samples collected from \mathcal{T}_1 to \mathcal{T}_{k-1} .

For GNNs, which have the capability to effectively harness and leverage the rich topological information embedded within the graph structure, the selection process of experience samples should consider not only the importance of samples in isolation but also their significance and influence at the topological level. A naive approach to incorporating topological information into experience is to sample nodes and their induced subgraph simultaneously:

$$(\mathcal{V}_k^{buf}, \mathcal{G}_k^{buf}) = \mathcal{S}(\mathcal{D}_k^{tr}, \mathcal{G}_k), \quad (2)$$

where $\mathcal{G}_k^{buf} = \mathcal{G}_k(\mathcal{V}_k^{buf})$ is the induced subgraph of \mathcal{G}_k with respect to the experience node set \mathcal{V}_k^{buf} . And $\mathcal{S}(\cdot)$ denotes the strategy used to select nodes and generate subgraph. With the

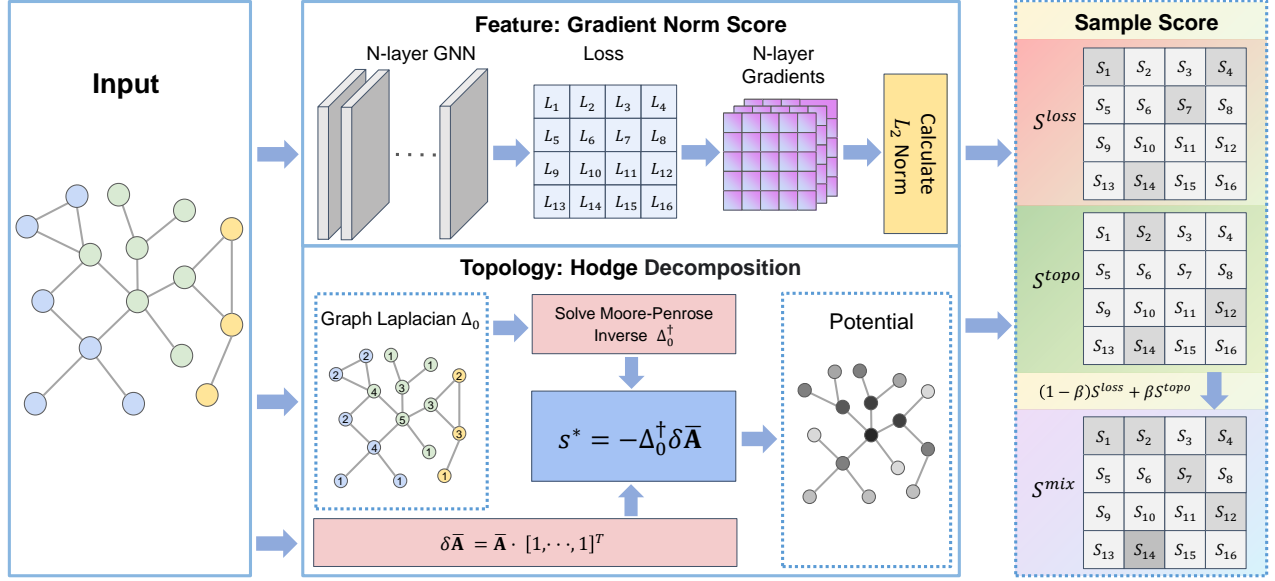


Figure 2: The complete node importance score calculation process for our FTF-ER. In the schematic diagram of Potential, the grayscale of nodes represents their importance, and the edges are only used to indicate the comparative results of importance. In the Sample Score stage, before mixing the two scores, they need to be normalized separately as shown in Eq. (18).

assistance of the topological information carried by the induced subgraph, the loss function for CGL can be defined as follows:

$$\mathcal{L} = \sum_{x_i \in \mathcal{D}_k^{tr}} l(f(x_i, \mathcal{G}_k; \theta), y_i) + \lambda \sum_{x_j \in V(\mathcal{B})} l(f(x_j, \mathcal{G}_k; \theta), y_j), \quad (3)$$

where \mathcal{G}_k is the subgraph stored in the buffer \mathcal{B} and $V(\mathcal{B})$ denotes the node set stored in \mathcal{B} . In other topology-based ER methods, \mathcal{G}_k is not necessarily an induced subgraph of $V(\mathcal{B})$, without loss of generality. For example in SSM [49], to obtain more topological information, the node set of \mathcal{G}_k includes not only $V(\mathcal{B})$ but also a subset of $\mathcal{N}(v)$ for each node v in $V(\mathcal{B})$, where $\mathcal{N}(v)$ represents the set of neighbors of node v in the graph.

In this paper, due to the acquisition of additional topological information reflected in the selection strategy of $V(\mathcal{B})$, we simply let $\mathcal{G}_k = \mathcal{G}(V(\mathcal{B}))$. Therefore, we do not need to bear the storage requirements of non-sample nodes in \mathcal{G}_k . The pipeline of the method we propose is illustrated in Figure 1.

3.3 Node Importance Score

To introduce our experience node selection strategy that integrates feature information and topological information, we first adopt the gradient norm (**GraNd**) score [28], which is used to compute the importance of nodes in the feature space. Next, we propose Hodge potential score (**HPS**) to calculate the importance scores of nodes at the topological level by HDG. Finally, we integrate the two importance scores to a weighted average score and provide the mixed node importance score for node selection. The complete computational process for calculating the node importance scores we propose is depicted in Figure 2.

3.3.1 Gradient Norm Score for Feature Importance. Inspired by [28], we introduce gradient norm score (**GraNd**) to measure the importance of nodes at the feature level. Intuitively, we can define a

sample's importance as its contribution to minimizing the model's loss function during training. Put simply, a sample is considered important if it helps reduce the loss of other samples when the model parameters are optimized using this particular sample. The importance of the training sample x_i can be formalized as follows:

$$I_i = \sum_{x_j \in X^{tr} - \{x_i\}} (l(f(x_j; \theta), y_j) - l(f(x_j; \theta'), y_j)), \quad (4)$$

where

$$\theta' = \theta - \eta \nabla_{\theta} l(f(x_i; \theta), y_i), \quad (5)$$

and η denotes the learning rate.

This definition intuitively represents the generalization ability of the selected sample, essentially measuring the sample's value in improving model predictions on other data. Simply put, we can estimate a sample's importance by calculating the gradient's norm it produces. In DNN models, updated via gradient descent, this gradient norm mirrors its effect on adjusting model parameters. Through theoretical validation [28], researchers approximate this effect by calculating the L_2 norm of the model gradients after training the respective node. GraNd is formally defined as follows:

$$S_i^{loss} = [S_1^{loss}, S_2^{loss}, \dots, S_{|X_k^{tr}|}^{loss}], \quad (6)$$

$$S_i^{topo} = \mathbb{E}_{\theta} \|\nabla_{\theta} l(f(x_i; \theta), y_i)\|_2.$$

The contribution of GraNd lies in its ability to make reasonable judgments on the importance of samples early in the training process, which aligns with the setting of incremental learning in CL. Therefore, we choose GraNd to calculate the importance of samples at the feature level, with the expectation that the selected samples can best fit the distribution of the entire dataset.

3.3.2 Hodge Potential Score for Topology Importance. We introduce the Hodge Potential Score (**HPS**), a novel measure of a node's topological importance in a graph. We discuss the motivation

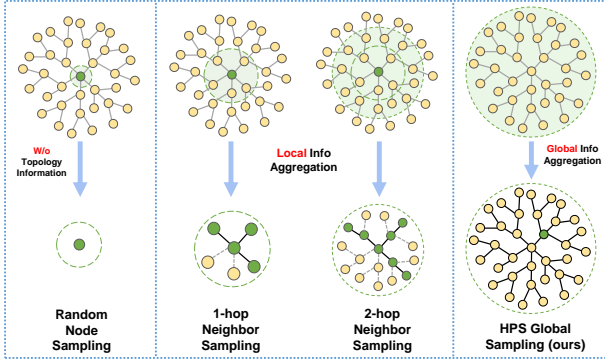


Figure 3: Acquiring topological information by random node sampling, SSM [49] with 1-hop, 2-hop neighbor sampling, and FTF-ER (ours). Green nodes indicate the ones selected to be added to the buffer, and bold solid lines represent the information flow between nodes during the sampling process.

behind proposing HPS. Unlike other topology-based ER methods or the commonly used PageRank [3] algorithm that acquire local topological information through neighboring node sampling, our HPS module uses the global ranking derived by Hodge decomposition on graphs (HDG) to measure the global topological importance of nodes, which can achieve more accurate global topological information. Additionally, in CGL, the storage overhead during model execution is also a crucial metric for ER methods. Applying HPS can circumvent the drawback of previous ER methods requiring the storage of neighboring nodes to obtain topological information.

To utilize HDG, we first introduce several key definitions of HDG used in our method. The complete descriptions of HDG is presented in *Appendix*. Let $\Omega^k(M)$ be a k -form on an n -dimensional smooth manifold M , d be the exterior derivative operator, and δ be the adjoint map of d , we provide the following definitions:

Definition 3.1 (Hodge Potential Score).

$$\Omega^0(\mathcal{G}) \triangleq \{s : \mathcal{V} \mapsto \mathbb{R}\}. \quad (7)$$

Definition 3.2 (Edge Flows).

$$\Omega^1(\mathcal{G}) \triangleq \{X : \mathcal{V} \times \mathcal{V} \mapsto \mathbb{R} | X(i, j) = -X(j, i), (i, j) \in \mathcal{E}\}. \quad (8)$$

Definition 3.3 (Gradient Operator). Let \mathbf{grad} be the gradient operator, $s_i, s_j \in \Omega^0(\mathcal{G})$, we have

$$(d_0 s)(i, j) \triangleq (\mathbf{grad} s)(i, j) \triangleq s_j - s_i, (i, j) \in \mathcal{E}. \quad (9)$$

Definition 3.4 (Negative Divergence Operator). Let w be the weight of an element in $\Omega^k(\mathcal{G})$, $w_i \in \Omega^0(\mathcal{G})$, $w_{ij} \in \Omega^1(\mathcal{G})$ and \mathbf{div} be the divergence operator, we have

$$(\delta_0 X)(i) \triangleq (-\mathbf{div} X)(i) = -\sum_j \frac{w_{ij}}{w_i} X(i, j). \quad (10)$$

Definition 3.5 (Graph Laplacian Operator).

$$\Delta_0 \triangleq \delta_0 d_0 \triangleq -\mathbf{div}(\mathbf{grad}). \quad (11)$$

To calculate HPS, we primarily make use of Definition C.7. Definition C.3 defines a function on graphs that maps a set of nodes \mathcal{V} to the real number field \mathbb{R} . This function is naturally suitable as a node importance scoring function and is referred to as Hodge potential score. Inspired by [17], we calculate HPS as follows:

$$\Delta_0 s = -\mathbf{div} \bar{Y}, \quad (12)$$

where \bar{Y} denotes inconsistent local rankings, which is consistent with the \mathbf{grad} in Definition C.7. In CGL, we simplify it to an anti-symmetric adjacency matrix \bar{A} on directed graphs, where

$$\bar{A}_{ij} = \begin{cases} 1, & \text{if } (i, j) \in \mathcal{E} \text{ and } (j, i) \notin \mathcal{E}, \\ -1, & \text{if } (j, i) \in \mathcal{E} \text{ and } (i, j) \notin \mathcal{E}, \\ 0, & \text{otherwise.} \end{cases} \quad (13)$$

For undirected graphs, $\bar{A} = A$.

The minimum norm solution of Eq. (12) is

$$s^* = -\Delta_0^\dagger \mathbf{div} \bar{A}, \quad (14)$$

where \dagger indicates a Moore-Penrose inverse.

By applying Definition C.6, we have

$$\mathbf{div} \bar{A} = \delta \bar{A} = \bar{A} \cdot [1, \dots, 1]^T. \quad (15)$$

And we have the common definition of the graph Laplacian:

$$\Delta_0 = D - A, \quad (16)$$

where $D = \text{diag}(\text{deg}(1), \dots, \text{deg}(n))$ and $\text{deg}(i)$ denotes the degree of node v_i .

By combining the above equations, we consolidate the formula for calculating HPS as follows:

$$S^{topo} = s^* = -\Delta_0^\dagger \delta \bar{A}. \quad (17)$$

It's obvious that for any node, HPS aggregates information from all other nodes. Figure 3 shows that our proposed HPS module achieves global topological information aggregation during node sampling, enhancing the accuracy of topological information and reducing buffer storage costs compared to the existing topology-based ER methods. Additionally, it is worth noting that the process of calculating HPS can be considered as a data preprocessing step, where the HPS of the various subdatasets after task partitioning can be computed before training. (Alternatively, HPS can be computed only once for the complete dataset.) This enables our approach to eliminate the need for training time when obtaining topological information, boosting training efficiency.

3.3.3 Fusion of GraNd and HPS. To fully leverage the comprehensive graph data, we integrate GraNd and HPS as follows. We adopt a weighted average approach to combine node importance scores S^{loss} and S^{topo} . Due to the different scales of the two types of scores S , it is necessary to perform min-max normalization on each of them before the combination:

$$\text{norm}(S) = \frac{S - \min(S)}{\max(S) - \min(S)}. \quad (18)$$

Then we define the mixed node importance score as follows:

$$S^{mix} = (1 - \beta) \text{norm}(S^{loss}) + \beta \text{norm}(S^{topo}), \quad (19)$$

where $\beta \in [0, 1]$ is a hyper-parameter used to adjust the emphasis of sampling. A higher β value indicates a stronger emphasis on the topological importance of nodes during sampling. Due to variations in the characteristics of different datasets, different β values are used during experimentation. A more detailed analysis of the values for β is presented in *Appendix*.

After calculating the mixed node importance scores, we can use these scores through two strategies: deterministic sampling or probabilistic sampling. The deterministic strategy directly sorts the nodes based on their scores and selects the top b nodes as the experience node set. In contrast, the probabilistic strategy uses the scores after standardization as a probability mass function: $p(i) =$

Table 1: Statistical information of four public graph datasets.

Dataset	Amazon Computers [26]	Corafull [4]	OGB-Arxiv [40]	Reddit [11]
# nodes	13,381	18,800	169,343	232,965
# edges	491,556	125,370	2,315,598	114,615,892
# classes	10	70	40	40
# tasks	5	35	20	20

$\frac{S_i^{mix}}{\sum_{j=0}^{|\mathcal{X}_k^{tr}|} S_j^{mix}}$. The experience node set is obtained by performing b rounds of sampling without replacement from the probability distribution defined by $p(i)$.

In conclusion, the experience selection strategy we propose can be described as follows: for each class in \mathcal{T}_k , we sample b nodes along with their induced subgraph $\mathcal{G}_k(\mathcal{V}_k^{buf})$, and then add them to buffer \mathcal{B} . To obtain the most accurate importance scores, we calculate the S^{loss} of \mathcal{T}_k and perform node selection after the completion of training for \mathcal{T}_k .

3.4 Algorithm Complexity Analysis

Time Complexity Analysis. To demonstrate the validity of our experiments regarding the algorithm’s runtime costs, we analyze the time complexity of FTF-ER from a complexity theory perspective. The majority of the time cost in our FTF-ER is concentrated in the calculation of HPS and GraNd. The calculation of HPS is completed in the preprocessing stage and does not contribute to the runtime cost. Besides, GraNd’s computation process requires a calculation for each node to be sampled, resulting in a complexity of $\mathcal{O}(n)$ when the number of sampled nodes is n , similar to ER-GNN. During the sampling stage, both FTF-ER and ER-GNN perform single sampling based on importance scores, resulting in a complexity of $\mathcal{O}(n)$. For the random neighbor sampling version of SSM [49], there is no importance score calculation stage. However, due to the need to sample neighbors for each node, the time complexity of the sampling stage in SSM is $\mathcal{O}(n^2)$. In summary, the total time complexity of FTF-ER and ER-GNN is $\mathcal{O}(n) + \mathcal{O}(n) = \mathcal{O}(n)$, while the total time complexity of SSM is $\mathcal{O}(n^2)$. This explains why the time cost of SSM is significantly higher than that of FTF-ER and ER-GNN during the experimental process.

Space Complexity Analysis. To validate the correctness of our experiments concerning buffer storage overhead, we analyze the space complexity of the buffer in FTF-ER from a complexity theory perspective. Similar to SSM [49], when the number of sampled nodes is n , the space complexity of the buffer in FTF-ER is $\mathcal{O}(n)$. However, since FTF-ER does not require introducing additional neighboring nodes, the additional space complexity of the buffer is $\mathcal{O}(1)$, while the additional space complexity of SSM remains $\mathcal{O}(n)$. Thus, we theoretically demonstrate that the space occupancy of our FTF-ER buffer is lower than that of SSM.

4 Experiments

4.1 Experimental Details

Datasets. We investigate multiple public datasets in the CGL field and select the four most representative graph node classification datasets for experimental exploration. These datasets have a wide coverage in terms of scale, content, and structure, enabling an effective evaluation of the generalizability of various CGL methods.

To enhance the difficulty of the experiments, following the setting of [48], we set the number of classes for each task to 2 on all datasets, thereby maximizing the length of the task sequence. In addition, to adapt to the majority of GNN backbones designed for undirected graphs, we standardize all datasets (including undirecting, removing weights, eliminating self-loops, and extracting the largest connected component). For each class, we divide the data into training, validation, and test sets in a ratio of 6:2:2. The statistical information of all the datasets is shown in Table 1.

Evaluation Metrics. There are two main types of evaluation metrics for CGL: average performance (AP) and average forgetting (AF) [25]. AP is used to measure the average testing performance of the model across all tasks, while AF can quantify the degree of forgetting on previously learned tasks. In this experiment, we adopt the average accuracy (AA) to quantify the performance: $AA = \frac{\sum_{i=1}^{|\mathcal{T}|} M_{\mathcal{T},i}^{acc}}{|\mathcal{T}|}$,

where $M^{acc} \in \mathbb{R}^{|\mathcal{T}| \times |\mathcal{T}|}$ denotes the accuracy matrix and $M_{i,j}^{acc}$ denotes model’s accuracy on task \mathcal{T}_j after learning task \mathcal{T}_i . Under

the setting of AP=AA, we have $AF = \frac{\sum_{i=1}^{|\mathcal{T}|-1} M_{\mathcal{T},i}^{acc} - M_{i,i}^{acc}}{|\mathcal{T}|-1}$. All the experiments are repeated 5 times, and the results are presented by means and standard deviations.

Baselines and backbones. We select our baselines from CGLB [48] including Elastic Weight Consolidation (EWC) [20], Learning without Forgetting (LwF) [22], Memory Aware Synapses (MAS) [1], Gradient Episodic Memory (GEM) [25], Experience Replay GNN (ER-GNN) [50], Topology-aware Weight Preserving (TWP) [24] and Sparsified Subgraph Memory (SSM) [49]. Additionally, we adopt joint training [6] as an approximation upper bound for model performance, and fine-tuning (without taking any measures against forgetting) as an approximation of the lower bound [9]. To validate the generalizability of the CGL methods, we implemented each CGL method on three mainstream GNN backbones: Graph Convolutional Networks (GCNs) [19], Graph Attention Networks (GATs) [37], and Graph Isomorphism Networks (GINs) [42]. Further implementation details are presented in *Appendix*.

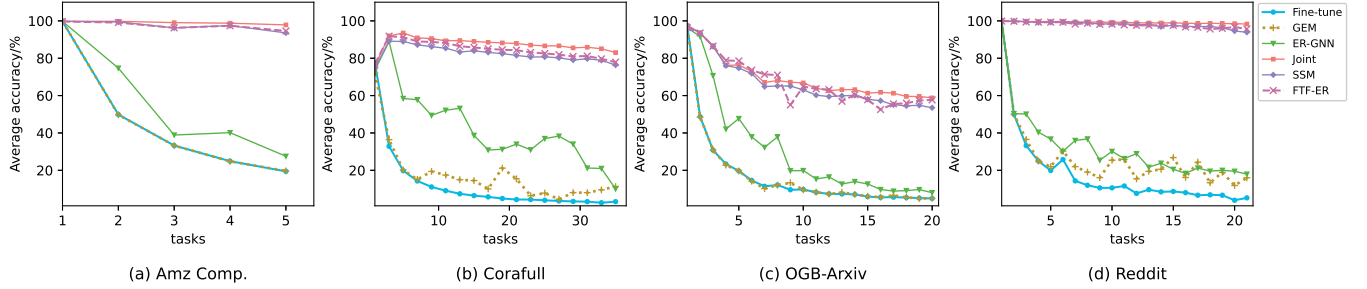
4.2 Comparisons with State-of-the-arts

We compare the performance of our method with other baselines on four public datasets. In order to introduce more randomness, we design two versions of our method based on different sampling methods: **FTF-ER-det.** in Table 2 refers to the FTF-ER method utilizing deterministic sampling, while **FTF-ER-prob.** presents utilizing probability distribution sampling. For a detailed description of these two sampling methods, please refer to Section 3.3.

The experimental results presented in Table 2 indicate that despite our proposed FTF-ER retains only subgraphs composed of a small number of nodes, it outperforms the current state-of-the-art method in the CGL field and performs similarly to the joint training method. This indicates that our FTF sampling strategy selects the most valuable nodes from the complete training dataset. Further analysis of the experimental data reveals that the vast majority of CGL methods perform poorly under the class-IL setting, with our FTF-ER significantly outperforming them. For the SSM method designed for the class-IL setting, our FTF-ER also outperforms by 1% to 3.6% in terms of AA and exhibits even better performance on AF, surpassing by 2% to 7.1%.

Table 2: Performance comparisons on 4 datasets under the class-IL setting (\uparrow higher indicates better performance).

CGL Methods	Amz Comp.		Corafull		OGB-Arxiv		Reddit	
	AA/% \uparrow	AF/% \uparrow	AA/% \uparrow	AF/% \uparrow	AA/% \uparrow	AF/% \uparrow	AA/% \uparrow	AF/% \uparrow
Fine-tune (soft lower bound)	19.4 \pm 0.0	-99.7 \pm 0.2	3.2 \pm 0.2	-95.7 \pm 0.1	4.9 \pm 0.0	-84.6 \pm 2.0	5.3 \pm 0.9	-94.3 \pm 2.1
EWC [20]	19.4 \pm 0.0	-99.6 \pm 0.2	36.2 \pm 9.1	-60.1 \pm 9.3	5.2 \pm 0.1	-92.0 \pm 0.2	12.3 \pm 2.8	-91.6 \pm 2.9
LwF [22]	19.4 \pm 0.0	-99.6 \pm 0.2	3.3 \pm 0.2	-95.3 \pm 0.3	4.9 \pm 0.1	-83.7 \pm 2.8	7.7 \pm 1.1	-87.7 \pm 1.8
MAS [1]	31.1 \pm 11.1	-46.4 \pm 24.8	28.6 \pm 5.2	-60.2 \pm 6.9	6.9 \pm 1.5	-23.5 \pm 10.9	13.1 \pm 4.9	-16.8 \pm 4.1
GEM [25]	19.7 \pm 0.8	-99.0 \pm 1.1	11.3 \pm 2.3	-85.1 \pm 2.6	5.0 \pm 0.1	-88.5 \pm 0.8	18.0 \pm 0.9	-84.4 \pm 1.0
ER-GNN [50]	27.5 \pm 5.1	-88.9 \pm 6.4	10.0 \pm 4.3	-80.7 \pm 4.7	7.5 \pm 0.8	-82.1 \pm 1.2	18.0 \pm 0.9	-84.4 \pm 1.0
TWP [24]	19.3 \pm 0.0	-99.6 \pm 0.1	42.2 \pm 5.0	-54.8 \pm 5.3	11.5 \pm 1.0	-75.8 \pm 4.1	9.7 \pm 1.6	-91.9 \pm 2.0
SSM [49]	93.6 \pm 0.8	-6.5 \pm 1.1	76.4 \pm 0.3	-10.6 \pm 0.4	54.7 \pm 2.6	-13.8 \pm 2.1	93.9 \pm 1.0	-4.6 \pm 1.2
Joint (soft upper bound)	97.8 \pm 0.1	-0.9 \pm 0.0	83.0 \pm 0.1	-2.1 \pm 0.2	58.8 \pm 0.3	-12.7 \pm 0.5	98.3 \pm 0.3	-0.4 \pm 0.2
FTF-ER-det. (Ours)	94.6\pm0.8	-4.5\pm1.1	77.5 \pm 0.1	-3.5\pm0.3	58.3\pm0.6	-10.5\pm0.5	95.2 \pm 0.7	-2.9 \pm 0.8
FTF-ER-prob. (Ours)	93.9 \pm 1.4	-5.3 \pm 1.9	77.9\pm0.1	-7.3 \pm 0.2	57.0 \pm 1.3	-11.8 \pm 1.7	95.7\pm0.6	-2.3\pm0.5

**Figure 4: Evolution of the AA throughout the learning process on the task sequences of four datasets.****Table 3: Ablation study on FTF-ER components.**

GrNd	HPS	Dataset	AA/% \uparrow	AF/% \uparrow
\times	\times	OGB-Arxiv	50.9 \pm 1.9	-15.0 \pm 1.2
\checkmark	\times	OGB-Arxiv	52.3 \pm 0.9	-12.5 \pm 1.0
\times	\checkmark	OGB-Arxiv	54.6 \pm 0.8	-7.0\pm1.6
\checkmark	\checkmark	OGB-Arxiv	58.3\pm0.6	-10.5 \pm 0.5

Furthermore, Figure 4 shows the decrease of AA for each ER-based CGL method as the number of tasks increases. Consistent with the results in Table 2, FTF-ER exhibits performance close to the upper bound throughout the entire learning process on all four datasets. This further indicates the effectiveness of our method in alleviating catastrophic forgetting issues. It is noteworthy that on the OGB-Arxiv dataset, FTF-ER exhibits large fluctuations in performance across task streams. This is attributed to the phenomenon of extreme class imbalance in the OGB-Arxiv dataset.

4.3 Ablation Studies

4.3.1 Effect of Components. To demonstrate the effectiveness of our proposed node sampling method that integrates feature-level and topological-level information, we construct three variants of our method and compare their performance with the complete FTF-ER on the OGB-Arxiv dataset. Table 3 summarizes the ablation experimental results of FTF-ER. We observe that all three sampling methods utilizing additional information outperformed random

Table 4: Comparisons on feature-level node selection.

Methods	Amazon Computers	
	AA/% \uparrow	AF/% \uparrow
FTF-ER (w/ Random)	91.0 \pm 3.5	-9.2 \pm 4.4
FTF-ER (w/ MF)	65.9 \pm 4.6	-41.1 \pm 5.7
FTF-ER (w/ CM)	85.8 \pm 5.1	-15.5 \pm 6.6
FTF-ER	94.6\pm0.8	-4.5\pm1.1

sampling, demonstrating that GrNd and HPS can accurately measure node importance. Furthermore, the best performance of the FTF (i.e. GrNd + HPS) sampling method, which combines the two scores, indicates that the fusion of feature-level information and topological-level information surpasses the approach of using only one of these types of information. However, it is noteworthy that the performance of FTF-ER (HPS only) is superior to that of the FTF-ER (GrNd + HPS) on the AF, while it is inferior on the AA. This suggests that topological information is more effective in enhancing the model’s memorization ability on the OGB-Arxiv dataset, and a model that integrates both types of information can provide more stable classification effectiveness.

4.3.2 Effect of GrNd. To demonstrate the effectiveness of gradient norm scores, we design three variants of FTF-ER, using random scores, mean of feature (MF) scores and coverage maximization (CM) scores (both of MF and CM are proposed in ER-GNN [50]) to calculate the feature-level importance of nodes. Table 4 presents that our original method achieves the best performance in both AA

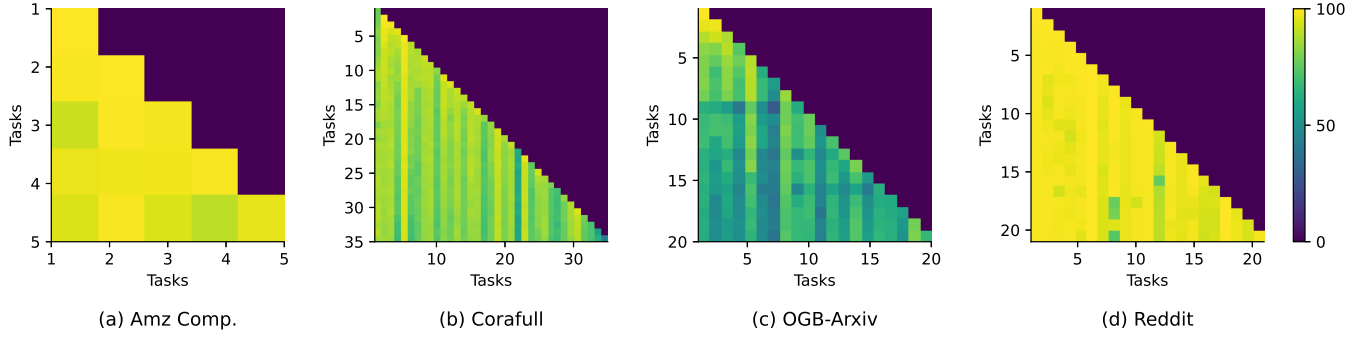


Figure 5: Visualization of the performance matrices of our FTF-ER method across four datasets.

Table 5: Comparisons on topological-level node selection.

Methods	Amazon Computers	
	AA/% \uparrow	AF/% \uparrow
FTF-ER (w/ Random)	93.5 \pm 2.0	-5.6 \pm 2.2
FTF-ER (w/ Random neighbor)	87.7 \pm 1.7	-13.3 \pm 2.3
FTF-ER (w/ Degree neighbor)	87.8 \pm 2.3	-13.3 \pm 2.9
FTF-ER	94.6\pm0.8	-4.5\pm1.1

Table 6: Comparisons of memory and time overheads of various ER-based CGL methods. * denotes that the methods utilize topological information.

Methods	Corafull		
	AA/% \uparrow	Buffer Memory/MB \downarrow	Training Time/sec \downarrow
ER-GNN[50]	10.0	128.65	1530.16
SSM[49] *	76.4	195.05	3614.25
GEM[25]	11.3	625.84	6176.56
FTF-ER *	77.9	128.94	1242.74

and AF metrics. This further demonstrates the rationale of choosing GraNd as the method for sampling feature-level information. Interestingly, **FTF-ER (w/ Random)** achieves the second-best performance, indicating that the ER-GNN method, which performs well in the task-IL setting, does not have the capability to generalize to the challenging class-IL setting.

4.3.3 Effect of HPS. To showcase the efficacy of Hodge potential scores, we design three additional variants for the method of extracting topological information to extract node topology information: random scores, random neighbor sampling, and degree-based neighbor sampling algorithms (both neighbor sampling algorithms are proposed in SSM [49]). Table 5 demonstrates that our original method achieves the best performance. This reveals that the global topological information collected by HPS is more helpful for node classification tasks compared to the local topological information collected through neighbor sampling used by SSM. Consequently, this further illustrates the rationale behind our choice of using HPS as a method for topological-level information sampling.

4.4 Computational Overhead

To demonstrate that our proposed method has lower computational overhead, we perform an experiment on the Corafull dataset with a

budget of 60 in order to investigate the buffer storage and training time cost associated with various ER-based CGL methods. In Table 6, we use **Buffer Memory** to indicate the size of the buffer after learning all tasks, and **Training Time** to represent the total time consumption of a training session.

Table 6 shows that our proposed method has nearly the same buffer memory overhead as ER-GNN that without providing topological information, and significantly lower than the SSM and GEM methods. This demonstrates that FTF-ER can reduce the storage overhead required for utilizing topological information. Furthermore, our FTF-ER method achieves the best overall training time among all ER-based CGL methods. This is mainly attributed to treating topological importance calculation as a preprocessing step, thereby reducing the time overhead during runtime.

4.5 Visualization

In order to better understand the dynamic performance of our FTF-ER method on different tasks, Figure 5 visualizes the performance matrix of average accuracy. Each cell in these matrices denotes the performance on task j (column) following the learning of task i (row). By looking at the matrices vertically, we can see how a specific task is gradually forgotten as training continues. By looking at the matrices horizontally, we can see how all the learned tasks perform at a given point in time. As training goes on, we notice that the colors of most tasks stay pretty much the same, matching the smooth curve of the FTF-ER method seen in Figure 4. This further validates the effectiveness of our proposed method in alleviating catastrophic forgetting issues of CGL.

5 Conclusion

In this paper, we propose FTF-ER to alleviate the catastrophic forgetting problem of CGL. From an overall perspective, FTF-ER proposes a highly complementary solution to fuse feature and topological information, thereby fully utilize the comprehensive graph data. By leveraging Hodge decomposition on graphs, we calculate the topological importance of nodes without additional storage space, and obtain more accurate global topological information compared to local neighbor sampling. We achieve state-of-the-art performance on accuracy and time efficiency in the challenging class-incremental learning setting, while maintaining comparable buffer storage costs to topology-agnostic methods. In future studies, we will devote efforts toward adapting FTF-ER to handle heterophilic graphs.

Acknowledgments

This work is supported by the National Key R&D Program of China under Grant No. 2020AAA0108600 and Guizhou Province Science and Technology Plan Project [2019]2505.

References

- [1] Rahaf Aljundi, Francesca Babiloni, Mohamed Elhoseiny, Marcus Rohrbach, and Tinne Tuytelaars. 2018. Memory aware synapses: Learning what (not) to forget. In *Proceedings of the European Conference on Computer Vision*. 139–154.
- [2] Rahaf Aljundi, Min Lin, Baptiste Goujaud, and Yoshua Bengio. 2019. Gradient based sample selection for online continual learning. *Advances in Neural Information Processing Systems* (2019).
- [3] Aleksandar Bojchevski, Johannes Gasteiger, Bryan Perozzi, Amol Kapoor, Martin Blais, Benedek Rózszerberczki, Michal Lukasik, and Stephan Günnemann. 2020. Scaling graph neural networks with approximate pagerank. In *ACM SIGKDD Conference on Knowledge Discovery and Data Mining*. 2464–2473.
- [4] Aleksandar Bojchevski and Stephan Günnemann. 2017. Deep gaussian embedding of graphs: Unsupervised inductive learning via ranking. *arXiv preprint arXiv:1707.03815* (2017).
- [5] Ozan Candogan, Ishai Menache, Asuman Ozdaglar, and Pablo A Parrilo. 2011. Flows and decompositions of games: Harmonic and potential games. *Mathematics of Operations Research* (2011), 474–503.
- [6] Rich Caruana. 1997. Multitask learning. *Machine Learning* (1997), 41–75.
- [7] Xu Chen, Junshan Wang, and Kunqing Xie. 2021. TrafficStream: A streaming traffic flow forecasting framework based on graph neural networks and continual learning. *arXiv preprint arXiv:2106.06273* (2021).
- [8] Mehrdad Farajtabar, Navid Azizan, Alex Mott, and Ang Li. 2020. Orthogonal gradient descent for continual learning. In *International Conference on Artificial Intelligence and Statistics*. 3762–3773.
- [9] Ross Girshick, Jeff Donahue, Trevor Darrell, and Jitendra Malik. 2014. Rich feature hierarchies for accurate object detection and semantic segmentation. In *Proceedings of the IEEE Conference on Computer Vision and Pattern Recognition*. 580–587.
- [10] Teng Guo, Feng Xia, Shihao Zhen, Xiaomei Bai, Dongyu Zhang, Zitao Liu, and Jiliang Tang. 2020. Graduate employment prediction with bias. In *Proceedings of the AAAI Conference on Artificial Intelligence*. 670–677.
- [11] Will Hamilton, Zhitao Ying, and Jure Leskovec. 2017. Inductive representation learning on large graphs. *Advances in Neural Information Processing Systems* (2017).
- [12] Yi Han, Shanika Karunasekera, and Christopher Leckie. 2020. Graph neural networks with continual learning for fake news detection from social media. *arXiv preprint arXiv:2007.03316* (2020).
- [13] Xiaoshuai Hao and Wanqian Zhang. 2024. Uncertainty-aware alignment network for cross-domain video-text retrieval. *Advances in Neural Information Processing Systems* 36 (2024).
- [14] Xiaoshuai Hao, Wanqian Zhang, Dayan Wu, Fei Zhu, and Bo Li. 2023. Dual alignment unsupervised domain adaptation for video-text retrieval. In *Proceedings of the IEEE/CVF conference on computer vision and pattern recognition*. 18962–18972.
- [15] Xiaoshuai Hao, Yi Zhu, Srikanth Appalaraju, Aston Zhang, Wanqian Zhang, Bo Li, and Mu Li. 2023. Mixgen: A new multi-modal data augmentation. In *Proceedings of the IEEE/CVF winter conference on applications of computer vision*. 379–389.
- [16] Tyler L Hayes and Christopher Kanan. 2020. Lifelong machine learning with deep streaming linear discriminant analysis. In *Proceedings of the IEEE Conference on Computer Vision and Pattern Recognition Workshops*. 220–221.
- [17] Xiaoye Jiang, Lek-Heng Lim, Yuan Yao, and Yinyu Ye. 2011. Statistical ranking and combinatorial Hodge theory. *Mathematical Programming* (2011), 203–244.
- [18] Peter Kingston and Magnus Egerstedt. 2011. Distributed-infrastructure multi-robot routing using a Helmholtz-Hodge decomposition. In *IEEE Conference on Decision and Control and European Control Conference*. 5281–5286.
- [19] Thomas N Kipf and Max Welling. 2016. Semi-supervised classification with graph convolutional networks. *arXiv preprint arXiv:1609.02907* (2016).
- [20] James Kirkpatrick, Razvan Pascanu, Neil Rabinowitz, Joel Veness, Guillaume Desjardins, Andrei A Rusu, Kieran Milan, John Quan, Tiago Ramalho, Agnieszka Grabska-Barwinska, et al. 2017. Overcoming catastrophic forgetting in neural networks. *Proceedings of the National Academy of Sciences* (2017), 3521–3526.
- [21] Dharshan Kumaran, Demis Hassabis, and James L McClelland. 2016. What learning systems do intelligent agents need? Complementary learning systems theory updated. *Trends in Cognitive Sciences* (2016), 512–534.
- [22] Zhizhong Li and Derek Hoiem. 2017. Learning without forgetting. *IEEE Transactions on Pattern Analysis and Machine Intelligence* (2017), 2935–2947.
- [23] Lek-Heng Lim. 2020. Hodge Laplacians on graphs. *Siam Review* (2020), 685–715.
- [24] Huihui Liu, Yiding Yang, and Xinchao Wang. 2021. Overcoming catastrophic forgetting in graph neural networks. In *Proceedings of the AAAI Conference on Artificial Intelligence*. 8653–8661.
- [25] David Lopez-Paz and Marc’Aurelio Ranzato. 2017. Gradient episodic memory for continual learning. *Advances in Neural Information Processing Systems* (2017).
- [26] Julian McAuley, Christopher Targett, Qinfeng Shi, and Anton Van Den Hengel. 2015. Image-based recommendations on styles and substitutes. In *ACM SIGIR Conference on Research and Development in Information Retrieval*. 43–52.
- [27] James L McClelland, Bruce L McNaughton, and Randall C O’Reilly. 1995. Why there are complementary learning systems in the hippocampus and neocortex: insights from the successes and failures of connectionist models of learning and memory. *Psychological Review* (1995), 419.
- [28] Mansheej Paul, Surya Ganguli, and Gintare Karolina Dziugaite. 2021. Deep learning on a data diet: Finding important examples early in training. *Advances in Neural Information Processing Systems* (2021), 20596–20607.
- [29] Sylvestre-Alvise Rebuffi, Alexander Kolesnikov, Georg Sperl, and Christoph H Lampert. 2017. Icarl: Incremental classifier and representation learning. In *Proceedings of the IEEE Conference on Computer Vision and Pattern Recognition*. 2001–2010.
- [30] David Rolnick, Arun Ahuja, Jonathan Schwarz, Timothy Lillicrap, and Gregory Wayne. 2019. Experience replay for continual learning. *Advances in Neural Information Processing Systems* (2019).
- [31] Andrei A Rusu, Neil C Rabinowitz, Guillaume Desjardins, Hubert Soyer, James Kirkpatrick, Koray Kavukcuoglu, Razvan Pascanu, and Raia Hadsell. 2016. Progressive neural networks. *arXiv preprint arXiv:1606.04671* (2016).
- [32] Franco Scarselli, Marco Gori, Ah Chung Tsoi, Markus Hagenbuchner, and Gabriele Monfardini. 2008. The graph neural network model. *IEEE Transactions on Neural Networks* (2008), 61–80.
- [33] Michael T Schaub, Austin R Benson, Paul Horn, Gabor Lippner, and Ali Jadbabaie. 2020. Random walks on simplicial complexes and the normalized Hodge 1-Laplacian. *SIAM Rev.* (2020), 353–391.
- [34] Michael T Schaub and Santiago Segarra. 2018. Flow smoothing and denoising: Graph signal processing in the edge-space. In *IEEE Global Conference on Signal and Information Processing*. 735–739.
- [35] Mariya Toneva, Alessandro Sordani, Remi Tachet des Combes, Adam Trischler, Yoshua Bengio, and Geoffrey J Gordon. 2018. An empirical study of example forgetting during deep neural network learning. *arXiv preprint arXiv:1812.05159* (2018).
- [36] Yiyang Tong, Santiago Lombeyda, Anil N Hirani, and Mathieu Desbrun. 2003. Discrete multiscale vector field decomposition. *ACM Transactions on Graphics* (2003), 445–452.
- [37] Petar Veličković, Guillem Cucurull, Arantxa Casanova, Adriana Romero, Pietro Lio, and Yoshua Bengio. 2017. Graph attention networks. *arXiv preprint arXiv:1710.10903* (2017).
- [38] Junshan Wang, Guojie Song, Yi Wu, and Liang Wang. 2020. Streaming graph neural networks via continual learning. In *ACM International Conference on Information & Knowledge Management*. 1515–1524.
- [39] Junshan Wang, Wenhao Zhu, Guojie Song, and Liang Wang. 2022. Streaming graph neural networks with generative replay. In *ACM SIGKDD Conference on Knowledge Discovery and Data Mining*. 1878–1888.
- [40] Kuansan Wang, Zhihong Shen, Chiyuan Huang, Chieh-Han Wu, Yuxiao Dong, and Anshul Kanakia. 2020. Microsoft academic graph: When experts are not enough. *Quantitative Science Studies* (2020), 396–413.
- [41] Mitchell Wortsman, Vivek Ramanujan, Rosanne Liu, Aniruddha Kembhavi, Mohammad Rastegari, Jason Yosinski, and Ali Farhadi. 2020. Supermasks in superposition. *Advances in Neural Information Processing Systems* (2020), 15173–15184.
- [42] Keyulu Xu, Weihua Hu, Jure Leskovec, and Stefanie Jegelka. 2018. How powerful are graph neural networks? *arXiv preprint arXiv:1810.00826* (2018).
- [43] Qianqian Xu, Qingming Huang, Tingting Jiang, Bowei Yan, Weisi Lin, and Yuan Yao. 2012. HodgeRank on random graphs for subjective video quality assessment. *IEEE Transactions on Multimedia* (2012), 844–857.
- [44] Jaehong Yoon, Saehoon Kim, Eunho Yang, and Sung Ju Hwang. 2019. Scalable and order-robust continual learning with additive parameter decomposition. *arXiv preprint arXiv:1902.09432* (2019).
- [45] Jaehong Yoon, Eunho Yang, Jeongtae Lee, and Sung Ju Hwang. 2017. Lifelong learning with dynamically expandable networks. *arXiv preprint arXiv:1708.01547* (2017).
- [46] Stella Yu. 2011. Angular embedding: A robust quadratic criterion. *IEEE Transactions on Pattern Analysis and Machine Intelligence* (2011), 158–173.
- [47] Qiao Yuan, Sheng-Uei Guan, Pin Ni, Tianlun Luo, Ka Lok Man, Prudence Wong, and Victor Chang. 2023. Continual graph learning: A survey. *arXiv preprint arXiv:2301.12230* (2023).
- [48] Xikun Zhang, Dongjin Song, and Dacheng Tao. 2022. Cglb: Benchmark tasks for continual graph learning. *Advances in Neural Information Processing Systems* (2022), 13006–13021.
- [49] Xikun Zhang, Dongjin Song, and Dacheng Tao. 2022. Sparsified subgraph memory for continual graph representation learning. In *IEEE International Conference on Data Mining*. 1335–1340.
- [50] Fan Zhou and Chengtai Cao. 2021. Overcoming catastrophic forgetting in graph neural networks with experience replay. In *Proceedings of the AAAI Conference on Artificial Intelligence*. 4714–4722.

A Algorithm

Algorithm 1 Framework of our FTF-ER.

Input: Task sequence $\mathcal{T} = \{\mathcal{T}_1, \mathcal{T}_2, \dots, \mathcal{T}_K\}$; Experience buffer \mathcal{B} ;
 Number of sampled nodes for each class b .
Output: A model $f(\cdot; \theta)$ that performs well on all tasks.

- 1: $\mathcal{B} \leftarrow (\emptyset, \emptyset)$
- 2: Initialize θ at random
- 3: **for** \mathcal{T}_i in \mathcal{T} **do**
- 4: Obtain training dataset $\mathcal{D}_i^{tr} = (\mathcal{V}_i^{tr}, \mathcal{G}_i)$ from \mathcal{T}_i
- 5: Extract experience nodes $V(\mathcal{B})$ and subgraph $\mathcal{G}_{\mathcal{B}}$ from \mathcal{B}
- 6: Compute $\mathcal{L}(f(\cdot; \theta), \mathcal{D}_i^{tr}, V(\mathcal{B}), \mathcal{G}_{\mathcal{B}})$ using Eq. (3)
- 7: $\theta \leftarrow \arg \min_{\theta} \mathcal{L}$
- 8: Compute $S^{mix}(f(\cdot; \theta), \mathcal{D}_i^{tr})$ using Eq. (19)
- 9: $\mathcal{V}_i^{buf} \leftarrow \text{Select}(\mathcal{V}_i^{tr}, S^{mix}, b)$
- 10: $\mathcal{B} \leftarrow (V(\mathcal{B}) \cup \mathcal{V}_i^{buf}, \mathcal{G}_{\mathcal{B}} \cup \mathcal{G}_i(\mathcal{V}_i^{buf}))$
- 11: **end for**

B Graph Neural Networks

Graph neural networks (GNNs) are deep learning models defined on a graph \mathcal{G} . At each layer of GNNs, nodes in \mathcal{V} update their hidden representations by aggregating and transforming information from their neighborhoods. The process of aggregation and transformation is accomplished by an update function that takes into account the hidden representations of the node and its adjacent nodes.

Formally, for each node v in \mathcal{V} , its hidden representation at the l -th layer of the GNN, denoted as $h_v^{(l)}$, is computed as follows:

$$h_v^{(l)} = U(h_v^{(l-1)}, h_u^{(l-1)}), \forall u \in \mathcal{N}(v), \quad (20)$$

where $U(\cdot)$ is a differentiable function and $\mathcal{N}(v)$ represents the set of neighbors of node v in the graph. $U(\cdot)$ takes the hidden representation of the current node $h_v^{(l-1)}$ and its neighboring nodes $h_u^{(l-1)}$ as inputs.

The graph convolutional network (GCN) [19] designs $U(\cdot)$ based on a first-order approximation of the spectra of the graph, which fixes the adjacency matrix \mathbf{A} . In the case of the attention-based GNN such as the graph attention network (GAT) [37], $U(\cdot)$ is designed based on pairwise attention. Furthermore, in [42], the authors highlight the performance limitations of GNNs and propose a new network called the graph isomorphism network (GIN). In our paper, the aforementioned three types of neural networks serve as the backbones of our FTF-ER.

C Theorem and Proof

C.1 Hodge Decomposition Theorem

Hodge decomposition theorem is a fundamental result in the theory of differential forms and Riemannian geometry. On a compact and oriented Riemannian manifold, the Hodge decomposition theorem states that any differential form can be uniquely decomposed into the sum of three components:

- **An exact form:** A differential form that is the exterior derivative of another form.

- **A co-exact form:** A differential form whose codifferential (adjoint of the exterior derivative) is zero.
- **A harmonic form:** A differential form that is both closed (its exterior derivative is zero) and co-closed (its codifferential is zero).

Let $\Omega^k(M)$ be a k -form on an n -dimensional smooth manifold M , d be the exterior derivative operator, and δ be the adjoint map of d . Then we can define the Hodge-Laplace operator:

Definition C.1 (Hodge-Laplace operator).

$$\Delta \triangleq d\delta + \delta d : \Omega^k(M) \mapsto \Omega^k(M). \quad (21)$$

Given the Definition C.1, we state the Hodge decomposition theorem as follows:

THEOREM C.2 (HODGE DECOMPOSITION THEOREM). *For any $\alpha \in \Omega^{k-1}(M)$, $\beta \in \Omega^{k+1}(M)$ and $\Delta\gamma = 0$, we have*

$$\omega \in \Omega^k(M) \Rightarrow \omega = d\alpha + \delta\beta + \gamma, \quad (22)$$

where $d\alpha$ is an exact k -form, $\delta\beta$ is a co-exact k -form and γ satisfying $\Delta\gamma = 0$ is also referred to as a harmonic form.

This decomposition is unique and orthogonal with respect to the L^2 inner product on the space of differential forms. The Hodge decomposition theorem has significant implications in various areas of mathematics and physics, including the study of cohomology, the theory of partial differential equations, and the formulation of Maxwell's equations in differential form language. Besides, this theorem allows us to categorize differential forms into three distinct types, each with its own physical interpretation:

- **An exact form $d\alpha$:** This differential form can be expressed as the gradient of a scalar field, making it particularly useful for describing potential energies associated with various fields. In physics, an exact form is commonly employed to represent electric potential energy or magnetic potential energy, providing valuable insights into the behavior of these fields.
- **A co-exact form $\delta\beta$:** A differential form that can be written as the curl of a vector field is classified as a coexact form. It plays a crucial role in describing circulation phenomena related to fields, such as magnetic flux in the context of magnetic fields. By utilizing a coexact form, physicists can effectively model and analyze the circulatory aspects of these fields.
- **A harmonic form γ :** Unlike an exact or a coexact form, a harmonic form is characterized by the absence of potential energies or circulations. It represents a state of equilibrium or scenarios devoid of sources or sinks. In the realm of physics, a harmonic form is frequently associated with fields that are free from sources, such as source-free electric fields or source-free magnetic fields. This form provides a framework for studying the behavior of fields in the absence of external influences.

C.2 Hodge Decomposition Theorem on Graphs

By defining several concepts on graphs, including d , Δ and δ when $k = 0$, we can generalize the Hodge decomposition theorem from its manifold version to graphs.

Definition C.3 (Hodge Potential Score).

$$\Omega^0(\mathcal{G}) \triangleq \{s : \mathcal{V} \mapsto \mathbb{R}\}. \quad (23)$$

Definition C.4 (Edge Flows).

$$\Omega^1(\mathcal{G}) \triangleq \{\mathcal{X} : \mathcal{V} \times \mathcal{V} \mapsto \mathbb{R} \mid \mathcal{X}(i, j) = -\mathcal{X}(j, i), (i, j) \in \mathcal{E}\}. \quad (24)$$

Definition C.5 (Gradient Operator). Let \mathbf{grad} be the gradient operator, $s_i, s_j \in \Omega^0(\mathcal{G})$, we have

$$(d_0 s)(i, j) \triangleq (\mathbf{grad} s)(i, j) \triangleq s_j - s_i, (i, j) \in \mathcal{E}. \quad (25)$$

Definition C.6 (Negative Divergence Operator). Let w be the weight of an element in $\Omega^k(\mathcal{G})$, $w_i \in \Omega^0(\mathcal{G})$, $w_{ij} \in \Omega^1(\mathcal{G})$ and \mathbf{div} be the divergence operator, we have

$$(\delta_0 \mathcal{X})(i) \triangleq (-\mathbf{div} \mathcal{X})(i) = -\sum_j \frac{w_{ij}}{w_i} \mathcal{X}(i, j). \quad (26)$$

Definition C.7 (Graph Laplacian Operator).

$$\Delta_0 \triangleq \delta_0 d_0 \triangleq -\mathbf{div}(\mathbf{grad}). \quad (27)$$

We note that we denote Δ_0 as the graph Laplacian operator. The proof that Δ_0 corresponds to the usual graph Laplacian operator is given in Section C.3.

Given the definitions above, we state the Hodge decomposition theorem on graphs for the case where $k = 0$ at first:

THEOREM C.8 (HODGE DECOMPOSITION THEOREM ON GRAPHS FOR $k = 0$). *Let \mathbf{Im} be the image set and \mathbf{ker} be the kernel set, we have*

$$\Omega^0(\mathcal{G}) = \mathbf{Im} d_0 \oplus \mathbf{Im} \delta_0 \oplus \mathbf{ker} \Delta_0. \quad (28)$$

In our paper, we employ the gradient field decomposition provided by the $k = 0$ version of the Hodge decomposition theorem on graphs to compute the topological importance of nodes. For the sake of theoretical completeness, we then describe the theorem for the case where $k \in \mathbb{N}$. To generalize the Hodge decomposition theorem on graphs for $k = 0$ to the case where $k \in \mathbb{N}$, we first denote K_k as the set of k -cliques on the graph. Then we have

$$\Omega^k(\mathcal{G}) \triangleq \{u : \mathcal{V}^{k+1} \mapsto \mathbb{R} \mid u(i_{\sigma(0)}, \dots, i_{\sigma(k)}) = \text{sign}(\sigma)u(i_0, \dots, i_k), \quad (29)$$

$$(i_0, \dots, i_k) \in K_{k+1}\}.$$

For $d_k : \Omega^k(\mathcal{G}) \mapsto \Omega^{k+1}(\mathcal{G})$ and $\delta_k : \Omega^k(\mathcal{G}) \mapsto \Omega^{k-1}(\mathcal{G})$, we define

$$(d_k u)(i_0, \dots, i_{k+1}) \triangleq \sum_{j=0}^{k+1} (-1)^{j+1} u(i_0, \dots, i_{j-1}, i_{j+1}, \dots, i_{k+1}), \quad (30)$$

and

$$(\delta_k u)(i_0, \dots, i_{k+1}) \triangleq \sum_{j=0}^{k+1} (-1)^j u(i_0, \dots, i_{j-1}, i_{j+1}, \dots, i_{k+1}). \quad (31)$$

Then we have

$$\Delta_k \triangleq \delta_k d_k + d_{k-1} \delta_{k-1}. \quad (32)$$

Given the definitions above, we state the Hodge decomposition theorem on graphs for $k \in \mathbb{N}$:

THEOREM C.9 (HODGE DECOMPOSITION THEOREM ON GRAPHS). *Let \mathbf{Im} be the image set and \mathbf{ker} be the kernel set, we have*

$$\Omega^k(\mathcal{G}) = \mathbf{Im} d_k \oplus \mathbf{Im} \delta_k \oplus \mathbf{ker} \Delta_k. \quad (33)$$

Theorem C.9 reveals that a graph signal can be decomposed into three orthogonal components:

- **Gradient component:** The gradient component represents the conservative or curl-free part of the graph signal. It can be expressed as the gradient of a potential function defined on the nodes of the graph. This means that the flow along any closed path in the graph sums up to zero. In other words, the gradient component captures the portion of the signal that exhibits no rotational behavior. It is analogous to the irrotational component in the continuous Hodge decomposition.
- **Curl component:** The curl component represents the rotational or divergence-free part of the graph signal. It can be expressed as the curl of a potential function defined on the edges of the graph. This means that the net flow out of any node in the graph is zero. The curl component captures the portion of the signal that exhibits rotational behavior but has no divergence.
- **Harmonic component:** The harmonic component is the part of the graph signal that is both gradient-free and divergence-free. It represents the signal's behavior that is not captured by either the gradient or the curl components. In other words, it is the part of the signal that is constant on connected components of the graph and has zero gradient and zero divergence.

These three components (i.e., gradient, curl, and harmonic) form a complete and orthogonal decomposition of the graph signal. They provide a way to analyze and understand the different aspects of the signal's behavior on the graph. The gradient component captures the conservative part, the curl component captures the rotational part, and the harmonic component captures the part that is neither conservative nor rotational. This decomposition is particularly useful in applications involving signal processing, data analysis, and machine learning on graph-structured data.

C.3 Graph Laplacian Operator

In this section, we give the proof that Δ_0 in our paper corresponds to the usual graph Laplacian operator for completeness, which may be found in [23].

PROOF. Let $s \in \Omega^1(\mathcal{G})$, we have

$$(\mathbf{grad} s)(i, j) = \begin{cases} s(j) - s(i), & \text{if } (i, j) \in \mathcal{E}, \\ 0, & \text{otherwise.} \end{cases} \quad (34)$$

Let a_{ij} be an element of the adjacency matrix \mathbf{A} , the gradient may be written as $(\mathbf{grad} s)(i, j) = a_{ij}(s(j) - s(i))$ and then

$$\begin{aligned} (\Delta_0 s)(i) &= -(\mathbf{div}(\mathbf{grad} s))(i) = -(\mathbf{div} a_{ij}(s(j) - s(i)))(i) \\ &= -\sum_{j=1}^n a_{ij}(s(j) - s(i)) = \xi_i s(i) - \sum_{j=1}^n a_{ij} s(j), \end{aligned} \quad (35)$$

where for any node v_i ($i = 1, \dots, n$), we define its degree as

$$\xi_i = \text{deg}(i) = \sum_{j=1}^n a_{ij}. \quad (36)$$

If we regard a function $s \in \Omega^1(\mathcal{G})$ as a vector $(s_1, \dots, s_n) \in \mathbb{R}^n$ where $s(i) = s_i$ and set $\mathbf{D} = \text{diag}(\xi_1, \dots, \xi_n) \in \mathbb{R}^{n \times n}$, then Eq. (35)

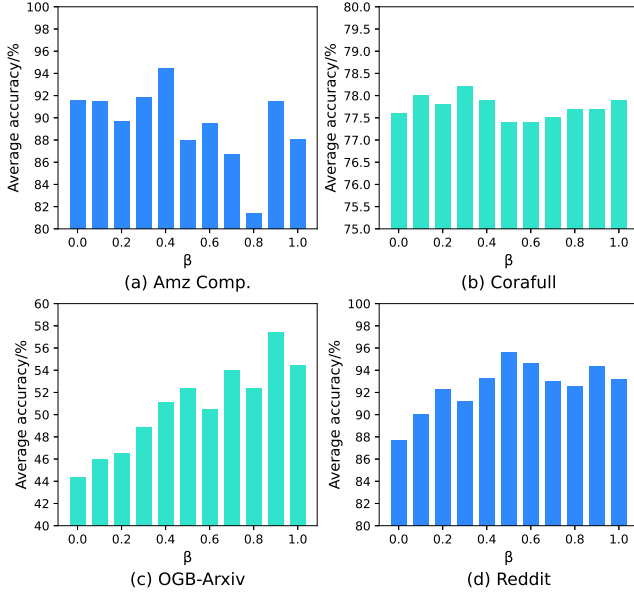


Figure 6: The influence of β on average accuracy.

becomes

$$\Delta_0 s = \begin{bmatrix} \xi_1 - a_{11} & -a_{12} & \cdots & -a_{1n} \\ -a_{21} & \xi_2 - a_{22} & \cdots & -a_{2n} \\ \vdots & \vdots & \ddots & \vdots \\ -a_{n1} & -a_{n2} & \cdots & \xi_n - a_{nn} \end{bmatrix} \begin{bmatrix} s_1 \\ s_2 \\ \vdots \\ s_n \end{bmatrix} = (\mathbf{D} - \mathbf{A})s. \quad (37)$$

So Δ_0 may be regarded as $\mathbf{D} - \mathbf{A}$, the usual definition of a graph Laplacian. \square

D Additional Experimental Details

D.1 Implementation Details

We use Adam optimizer to optimize the models, setting the initial learning rate to 0.005 and the number of training epochs to 200 on all datasets. The regularizer hyper-parameter for EWC [20], MAS and TWP is always set to 10,000. And β for TWP [24] is set to 0.01. For those experience replay baselines, i.e., GEM [25], ER-GNN [50] and SSM [49], we set the buffer size for each class to be 60, 60, 400, 100 for Amazon Computers, Corafull, OGB-Arxiv, and Reddit, respectively. For our method, we choose a buffer size that is the same as that of other methods and select a suitable β from [0.0, 0.25, 0.5, 0.75, 1.0] for different datasets. Additionally, we set the structure of all backbones as a 2-layer network with a hidden layer dimension of 256 for fairness. Finally, due to the abundance of experimental results for each method across all the three backbones, we only present the best results of each method on each dataset.

D.2 Sensitivity of Hyper-parameter

To analyze the sensitivity of our method to the value of the hyper-parameter β , we demonstrate the influence of β on AA using the total four datasets. In this experiment, we further divide β into [0.0, 0.1, 0.2, 0.3, 0.4, 0.5, 0.6, 0.7, 0.8, 0.9, 1.0] to observe its effects more

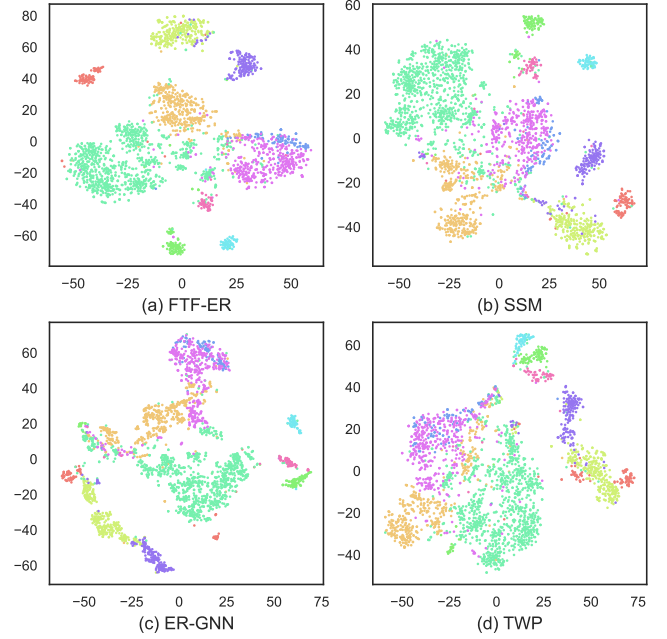


Figure 7: 2-D t-SNE projections of embeddings in four models. The nodes with different labels are represented by dots in different colors.

carefully. Figure 6 displays that the value of β has different effects on different datasets. For example, on the Amazon Computers dataset, it leads to approximately 14% performance fluctuation, while on the Corafull dataset, it only leads to about 0.8% fluctuation. Further analysis of the experiments reveals that the peak consistently occurs at the middle position on all datasets, which further confirms the effectiveness of our feature-topology fusion sampling.

D.3 Qualitative Analysis

In order to demonstrate the effectiveness of the node representations learned by FTF-ER, we conduct a qualitative analysis on the Amazon Computers dataset. For this purpose, we generate a series of standard t-SNE 2D projected plots of node representations to reinforce this analysis. We select the complete test data set containing 5 tasks and 10 classes for demonstration, to analyze the overall performance of each model after undergoing the complete continual learning process. Given FTF-ER's ability to differentiate between the importance of nodes at the feature and topological levels, we anticipate that nodes sharing the same labels will be positioned closely in the projection space, indicating similar representation vectors. Figure 7 visualizes the hidden layer representations of four CGL methods, namely FTF-ER, SSM [49], ER-GNN [50], and TWP [24]. Experimental results show that FTF-ER exhibits a clearer separation of nodes from distinct communities compared to alternative methods. The nodes with different labels are represented by dots in different colors. This showcases the capability of our FTF-ER in capturing distinctions among nodes within diverse communities through the gathered node information.